Hindawi Publishing Corporation
International Journal of Polymer Science
Volume 2014, Article ID 243895, 8 pages
http://dx.doi.org/10.1155/2014/243895

Research Article

Numerical Model of Radical Photopolymerization Based on Interdiffusion

Shuhei Yoshida, Yosuke Takahata, Shuma Horiuchi, Hiroyuki Kurata, and Manabu Yamamoto

Department of Applied Electronics, Tokyo University of Science, 6-3-1 Niijuku, Katsushika-ku, Tokyo 125-8585, Japan

Correspondence should be addressed to Shuhei Yoshida; syoshida@rs.tus.ac.jp

Received 25 July 2014; Revised 15 October 2014; Accepted 5 November 2014; Published 10 December 2014

Academic Editor: Sergi Gallego

An accurate reaction model is required to analyze the characteristics of photopolymers. For this purpose, we propose a numerical model for radical photopolymerization. In the proposed model, elementary reactions such as initiation, propagation, and termination are considered, and we assume interdiffusion for each component in the material. We analyzed the diffraction characteristics of a radical photopolymer based on the proposed interdiffusion model with the beam propagation method. Moreover, we also performed hologram-recording experiments and evaluated the diffraction characteristics of the photopolymer medium. By comparing the numerical and experimental results, medium parameters such as reaction rate and diffusion coefficient can be estimated. We confirmed that the interdiffusion model can reproduce the experimental results and showed that the medium parameters affect the diffraction characteristics.

1. Introduction

Photopolymers are photoactive organic materials with high diffraction efficiency and are low-cost and stable materials with high dynamic range; thus, photopolymers are widely used in recording holograms. The photopolymerization reaction is complex; therefore, an accurate reaction model is needed for understanding the recording mechanism and analyzing the photopolymer characteristics.

Zhao and Mouroulis proposed a one-dimensional diffusion model for photopolymers [1] with some numerical results. In their simulation, the holographic grating was assumed to have a periodic structure, and the numerical analysis was based on Fourier series expansion. Following Zhao and Mouroulis, several researchers proposed reaction models based on diffusion [2–9]. In these models, the broadening of the polymer chain [2–4], shrinkage of the medium [6, 7], and dark reaction [7–9] were considered. Additionally, reaction parameters, such as kinetic constants, were estimated by using experimental results [10–15]. In these studies, models with one-dimensional structure were assumed. Therefore, it is difficult to analyze diffraction characteristics, such as angular selectivity and multiplexing, in detail. In this study, we expand the diffusion model to two dimensions to improve the analysis of diffraction characteristics. The model introduces elementary reactions such as initiation, propagation, and termination. By introducing the primary reactions, we can estimate the kinetic constants of each component.

We simulated the formation of the holographic grating based on the two-dimensional interdiffusion model and used the beam propagation method (BPM) [16] to analyze the diffraction characteristics. Based on previous works [17, 18], BPM is considered effective for analyzing diffraction characteristics. By using BPM, we can analyze the diffraction characteristics of the complex holographic grating. Moreover, we also performed hologram-recording experiments. By comparing the numerical and experimental results, we estimated medium parameters, such as reaction rate and diffusion coefficient, and clarified how the medium parameters affect the diffraction characteristics.

2. Numerical Model

2.1. Chemical Kinetics. We discuss the chemical kinetics of radical polymerization and construct the reaction model.

Radical polymerization proceeds following elementary reactions such as

$$\mathrm{I} \xrightarrow{k_d} 2\mathrm{R}^{\bullet} \tag{1}$$

$$\mathrm{R}^{\bullet} + \mathrm{M} \xrightarrow{k_i} \mathrm{R} - \mathrm{M}^{\bullet} \left(\equiv \mathrm{P}^{\bullet}\right), \tag{2}$$

$$\mathrm{P}^{\bullet} + \mathrm{M} \xrightarrow{k_p} \mathrm{P}^{\bullet}, \tag{3}$$

$$\mathrm{P}^{\bullet} + \mathrm{P}^{\bullet} \xrightarrow{k_{tc}} \mathrm{P} \quad (\text{by combination})$$

$$\mathrm{P}^{\bullet} + \mathrm{P}^{\bullet} \xrightarrow{k_{td}} 2\mathrm{P} \quad (\text{by disproportionation}), \tag{4}$$

$$\mathrm{P}^{\bullet} + \mathrm{A} \xrightarrow{k_{tr}} \mathrm{P} + \mathrm{A}^{\bullet},$$

where I, $\mathrm{R}^{\bullet}$, $\mathrm{P}^{\bullet}$,M, and P are the initiator, primary radical, propagating radical, monomer, and polymer, respectively, and k_d, k_i, k_p, k_{tc}, k_{td}, and k_{tr} are the reaction rate constants. Equations (1)–(4) denote the chain initiation, propagation, termination, and chain transfer, respectively. Primary radicals are produced by the decomposition of the initiators via exposure. By adding dyes to the photopolymer, the spectral sensitivity of the initiator can be adjusted. Then, the molecular weight of the propagating radical increases by binding monomers. Two propagating radicals are bound with each other. At this stage, there are two termination pathways. One is the combination reaction and the other is the disproportionation reaction. In general, radical polymerization proceeds with the abovementioned elementary reactions. Chain transfer was not considered for simplicity. Figure 1 shows the reaction path of the radical polymerization described above.

We assume that the initiation rate is proportional to the intensity of exposure

$$k_d \propto I_0(\mathbf{r}), \tag{5}$$

and $I_0(\mathbf{r})$ is expressed as

$$I_0(\mathbf{r}) = I_0\left[1 + V\cos\left(\mathbf{K_g}\cdot\mathbf{r}\right)\right], \tag{6}$$

where I_0 is the exposure intensity, V is the visibility of the interference pattern, and $\mathbf{K_g}$ is the grating vector. $\mathbf{K_g}$ is defined as the wave vector difference of the signal and reference beam in the medium.

2.2. Interdiffusion Model. In this section, we explain the interdiffusion model. Figure 2 shows the phenomenological reaction model for photopolymers.

The signal and reference beams generate the interference pattern in the medium, and polymerization proceeds in the bright area. Polymerization causes concentration gradients; therefore, each component diffuses in response to the gradients. Because the refractive index of each component differs, the hologram is recorded as the refractive index distribution in the photopolymer medium.

In this study, we assumed that the photopolymerization proceeds via the diffusion and reaction of each component. The diffusion and reaction of each component can be described as a generalized mass action system [19–21] using the formulation

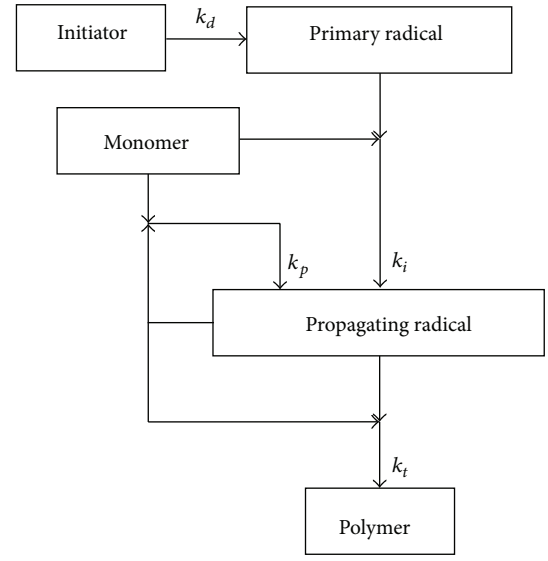

Figure 1: Reaction path of radical polymerization.

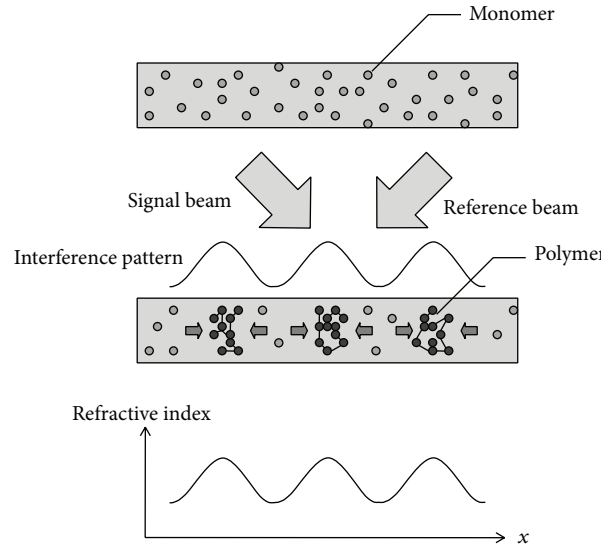

Figure 2: Photopolymer reaction model.

$$\frac{\partial X_i}{\partial t} = \sum_{j=1}^{N} \alpha_{ij} \prod_{k=1}^{d} X_j^{g_{ijk}} - \sum_{j=1}^{N} \beta_{ij} \prod_{k=1}^{d} X_j^{h_{ijk}} + \nabla \cdot \left(D_i \nabla X_i\right), \tag{7}$$

where d is the number of components and subscript $i = 1, 2, \ldots, 5$ represents the initiator, primary radical, propagating radical, monomer, and polymer, respectively. N represents the number of production reaction terms. X_i and D_i are the concentration and diffusion coefficients of each component, respectively. α_i and β_i are the reaction rate constants, and the terms g_{ijk} and h_{ijk} represent the interactive effect between X_i and X_j. The first and second term of the right-hand side of the equation indicate the increase and decrease of the material, and the third term denotes diffusion.

Table 1: Parameters of the interdiffusion model ($j = 1$).

i	α_{i1}	g_{i11}	g_{i12}	g_{i13}	g_{i14}	g_{i15}	β_{i1}	h_{i11}	h_{i12}	h_{i13}	h_{i14}	h_{i15}
1	0	0	0	0	0	0	k_d	1	0	0	0	0
2	$2k_d$	1	0	0	0	0	k_i	0	1	0	1	0
3	k_i	0	1	0	1	0	k_t	0	0	2	0	0
4	0	0	0	0	0	0	k_i	0	1	0	1	0
5	k_t	0	0	2	0	0	0	0	0	0	0	0

Table 2: Parameters of the interdiffusion model ($j = 2$).

i	α_{i2}	g_{i21}	g_{i22}	g_{i23}	g_{i24}	g_{i25}	β_{i2}	h_{i21}	h_{i22}	h_{i23}	h_{i24}	h_{i25}
1	0	0	0	0	0	0	0	0	0	0	0	0
2	0	0	0	0	0	0	0	0	0	0	0	0
3	0	0	0	0	0	0	0	0	0	0	0	0
4	0	0	0	0	0	0	k_p	0	0	1	1	0
5	0	0	0	0	0	0	0	0	0	0	0	0

We also assumed that the polymer does not diffuse in the medium. Since molecular weight of the polymer chains is high, the polymer hardly diffuses on the short time-scale. However, on the long timescale, diffusion of the polymer might cause degradation of the hologram because of collapse of the grating form. The parameters in (7) are listed in Tables 1 and 2. The reaction rates of each component are decided by the reaction kinetics of the elementary reactions.

We estimate parameters, such as reaction rate constants and diffusion coefficients, by using experimental results. The refractive index distribution of the medium is determined by using the Lorentz-Lorenz equation

$$n = \sqrt{\frac{1 + 2\phi}{1 - \phi}}, \qquad \phi = \sum_i \frac{n_i^2 - 1}{n_i^2 + 2}\phi_i, \tag{8}$$

where ϕ_i is the volume fraction and n_i is the refractive index of the ith component. The volume fraction ϕ_i is

$$\phi_i = \frac{w_i/d_i}{\sum_i w_i/d_i}, \tag{9}$$

where w_i is the mass fraction and d_i is the density of each component. Equation (7) is discretized for numerical analysis, and it is formulated with the alternating direction implicit method. In the simulation, materials cannot move over the boundary; therefore we employed the Neumann boundary condition

$$\frac{\partial X_i}{\partial n} = 0, \quad \mathbf{r} \in \partial\Omega, \tag{10}$$

where n is the normal unit vector at the boundary.

3. Numerical and Experimental Results

3.1. Experimental Setup. Figure 3 shows the experimental configuration for evaluating the photopolymer medium.

We used the second harmonic of yttrium aluminum garnet laser (532 nm) for recording and the laser diode (670 nm) for readout. We performed two-beam interference recording using the 532 nm laser and monitored the change in diffraction efficiency in real time using the 670 nm laser. The signal and reference beam formed a 60° angle. By using a laser of a different wavelength for readout, we could monitor the diffraction characteristics in real time. The experimental conditions are listed in Table 3.

Table 3: Experimental conditions.

Exposure intensity I_0	10 mW/cm^2
Incident angle of signal θ_s	30°
Incident angle of reference θ_r	−30°
Wavelength for recording λ	532 nm
Medium thickness	25 μm
Visibility	1.0
Beam diameter for recording φ	5 mm
Beam diameter for monitor φ	1 mm

Table 4: Composition and properties of the photopolymer medium.

Component	Mass fraction	Density [g/cm^3]	Refractive index
Initiator	5.0 wt%	1.078	1.525 (in solvent)
Monomer	45 wt%	1.183	1.485
Polymer	—	1.277	1.518
Solvent	25 wt%	1.106	1.502
Plasticizer	25 wt%	0.965	1.430

We used a highly sensitive ($S > 10\,\text{cm}^2/\text{J}$), 25 μm thick, photopolymer medium tin for the experiment. The sample medium was fabricated by injecting the photopolymer between 1 mm glass substrates. The shrinkage ratio of the medium is 0.1% order. The composition and property of the photopolymer are listed in Table 4. This sample was provided by Daicel Corporation. Detailed information of the material cannot be revealed because of nondisclosure agreement.

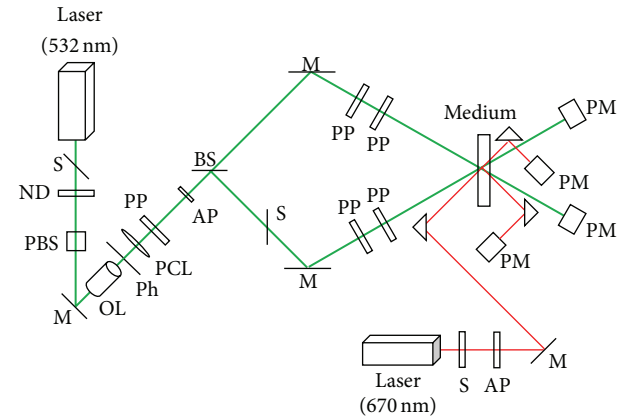

BS: beam splitter
PP: polarizing plate
PM: power meter
AP: aperture
M: mirror
OL: object lens
S: shutter
PBS: polarization beam splitter
ND: ND filter
PCL: plano-convex lens
Ph: pinhole

Figure 3: Experimental configuration.

3.2. Simulation Scheme. We used BPM [10] for the numerical analysis of the diffraction characteristics of the holographic gratings. BPM is based on steady-state Maxwell's equations. The electromagnetic field is computed with the following equation:

$$2jn_r k_0 \frac{\partial \phi}{\partial z} - \frac{\partial^2 \phi}{\partial z^2} = P\phi,$$

$$P = \begin{cases} \dfrac{\partial^2}{\partial x^2} + k_0^2\left(n^2 - n_r^2\right) & (\mathrm{TE}), \\ n^2 \dfrac{\partial}{\partial x}\left(\dfrac{1}{n^2}\dfrac{\partial}{\partial x}\right) + k_0^2\left(n^2 - n_r^2\right) & (\mathrm{TM}), \end{cases} \tag{11}$$

where n_r is the reference refractive index, k_0 is the wave number in free space, and n is the refractive index of the medium. This equation is developed from steady-state Maxwell's equations and slowly varying the envelope approximation. In the conventional BPM, the $\partial^2\varphi/\partial z^2$ term is neglected to transform (11) into a parabolic partial differential equation. In this study, however, we do not neglect the $\partial^2\varphi/\partial z^2$ term; (11) is split into forward and backward wave equations and is expanded as high-order Pade series for accurate calculations [22]. The transparent boundary condition [23] is adopted as the absorption boundary condition. The electromagnetic field is calculated by numerically solving (11) in the z-direction.

Figure 4 shows the virtual analytical region of the numerical analysis. The holographic grating is located in the analytical region, which is surrounded by the absorption boundary.

The incident plane wave enters the analytical region from on the left side. The incident beam is diffracted by the holographic grating, and the diffracted beam is separated from the transmitting beam using the fast Fourier transform. Diffraction efficiency is defined as the ratio of the intensity of the diffracted and incident beam.

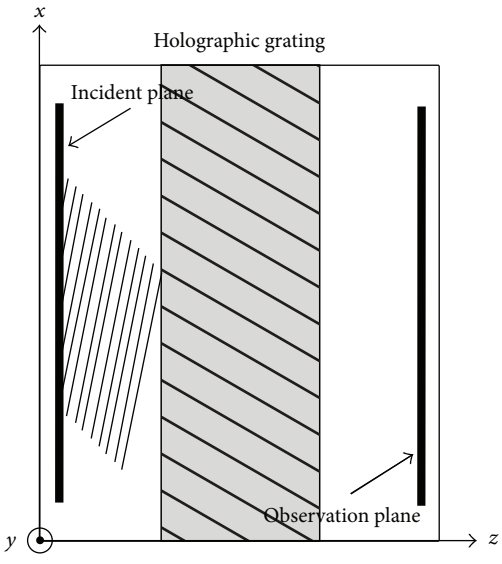

Figure 4: Analytical region.

3.3. Parameter Fitting. We used the Levenberg-Marquardt algorithm (LMA) [24, 25] for parameter fitting. LMA is a nonlinear numerical optimization method and combines the Gauss-Newton algorithm and Gradient descent. LMA searches for parameters that minimize the assessment function. Generally, chi-square distribution χ^2 is used as the assessment function

$$\chi^2(\mathbf{a}) = \sum_i \left[\frac{y_i - f(x_i; \mathbf{a})}{\sigma_i}\right]^2 = \left\|\mathbf{y} - \mathbf{f}(\mathbf{a})\right\|^2, \tag{12}$$

where $\mathbf{a} = (k_d, k_i, k_p, k_t, D_1, D_2, D_3, D_4)$ is the parameter vector, x_i and y_i are the given independent and dependent variables, σ_i is the standard deviation, f is the model function, $\|\|$ represents the Euclidean distance, $\mathbf{y} = (y_1/\sigma_1, y_2/\sigma_2, \ldots)$, and $\mathbf{f} = (f(x_1; \mathbf{a})/\sigma_1, f(x_2; \mathbf{a})/\sigma_2, \ldots)$. LMA is used iteratively. The increment of parameters $\boldsymbol{\delta}$ is obtained by solving the following system of linear equations:

$$\begin{aligned}\left[\mathbf{H} + \lambda \operatorname{diag}(\mathbf{H})\right]\boldsymbol{\delta} &= \nabla\chi^2(\mathbf{a}) \\ &= \mathbf{J}^T\chi^2(\mathbf{a}) \\ &= -2\left[\mathbf{y} - \mathbf{f}(\mathbf{a})\right]\cdot\frac{\partial\mathbf{f}(\mathbf{a})}{\partial\mathbf{a}^T},\end{aligned} \tag{13}$$

where represents the inner product, $\mathbf{J}$ is the Jacobian matrix, $\mathbf{H}$ is the Hessian matrix

$$\mathbf{H} = \begin{bmatrix} \dfrac{\partial^2\chi^2(\mathbf{a})}{\partial a_1^2} & \dfrac{\partial^2\chi^2(\mathbf{a})}{\partial a_1\partial a_2} & \cdots & \dfrac{\partial^2\chi^2(\mathbf{a})}{\partial a_1\partial a_n} \\ \dfrac{\partial^2\chi^2(\mathbf{a})}{\partial a_2\partial a_1} & \dfrac{\partial^2\chi^2(\mathbf{a})}{\partial a_2^2} & \cdots & \dfrac{\partial^2\chi^2(\mathbf{a})}{\partial a_2\partial a_n} \\ \vdots & \vdots & \ddots & \vdots \\ \dfrac{\partial^2\chi^2(\mathbf{a})}{\partial a_n\partial a_1} & \dfrac{\partial^2\chi^2(\mathbf{a})}{\partial a_n\partial a_2} & \cdots & \dfrac{\partial^2\chi^2(\mathbf{a})}{\partial a_n^2} \end{bmatrix}, \tag{14}$$

and λ is a fudge factor. Typically, the second-order derivative terms of the matrix elements in the Hessian matrix are neglected for simplicity and stability [26]

$$\begin{aligned}\frac{\partial^2\chi^2(\mathbf{a})}{\partial a_i\partial a_j} &= 2\left[\frac{\partial\mathbf{f}(\mathbf{a})}{\partial a_i}\cdot\frac{\partial\mathbf{f}(\mathbf{a})}{\partial a_j} - \left[\mathbf{y} - \mathbf{f}(\mathbf{a})\right]\cdot\frac{\partial^2\mathbf{f}(\mathbf{a})}{\partial a_i\partial a_j}\right] \\ &\approx 2\frac{\partial\mathbf{f}(\mathbf{a})}{\partial a_i}\cdot\frac{\partial\mathbf{f}(\mathbf{a})}{\partial a_j}.\end{aligned} \tag{15}$$

Then, the Hessian matrix can be approximated as

$$\mathbf{H} \approx \mathbf{J}^T\mathbf{J}. \tag{16}$$

Figure 5 shows the LMA procedure.

3.4. Results. Figure 6 shows the time variation of the diffraction efficiency. Solid and dashed curves express the experimental and simulation results, respectively. Horizontal and vertical axes correspond to the exposure time and diffraction efficiency. Diffraction efficiency increased at the start of exposure and saturated with time, and it was almost saturated after 100 s. There are differences between the experimental and simulation results. By focusing on the short-time scale after the start of exposure ($t < 5$ s), we identified an occurrence of a minor peak in the experimental results. This phenomenon may be caused by the refractive index contrast transition [27].

Medium parameters are estimated by fitting the experimental and simulation results using LMA. The estimated medium parameters are listed in Table 5.

The root mean squared error (RMSE) between experimental and simulation results is 9.454×10^{-3}. The diffusion

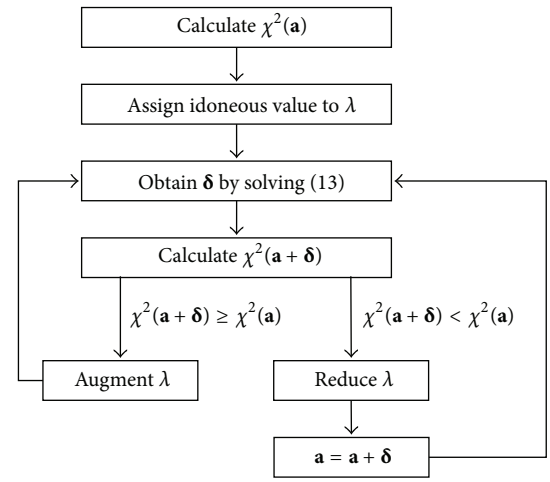

Figure 5: LMA procedure.

Table 5: Estimated medium parameters.

Parameter	Value
k_d	7.277 ± 5.307 ($\times 10^{-2}$) [1/s]
k_i	1.576 ± 3.007 [1/s]
k_p	1.463 ± 0.1661 ($\times 10^{-1}$) [1/s]
k_t	4.916 ± 1.755 ($\times 10^{-1}$) [1/s]
D_1	7.143 ± 9.668 ($\times 10^{-12}$) [cm^2/s]
D_2	~0 [cm^2/s]
D_3	~0 [cm^2/s]
D_4	7.259 ± 20.83 ($\times 10^{-12}$) [cm^2/s]

coefficient of the primary radical $D_2 \sim 0$ indicates that the primary radical reacts with the monomer immediately after production. Furthermore the propagating radical $D_3 \sim 0$ indicates that diffusion of propagating radical is inhibited by a rapid increase in molecular weight of polymer chains by propagation. Next, we evaluate the angular selectivity based on the estimated parameters. Figure 7 shows the experimental and simulation angular selectivity after 100 s exposure time. The horizontal axis $\Delta\theta$ expresses the angle gap between the recording and readout angle.

The full-width-at-half-maximum of the experimental data is 2.44×10^{-3} rad. Simulation well reproduced the experimental results. The experimental results were also reproduced with a sinc^2-like function, which is expected from coupled wave analysis (CWA) [28]. The refractive index modulation Δn, which is estimated from the experimental results with CWA, is $\Delta n = (6.018 \pm 0.05127) \times 10^{-3}$. Bragg nulls clearly occur in the experimental results and thus absorption by the medium is low [29]. The simulation results and CWA slightly differ from the experimental results. This can be caused by the difference between each grating form.

The space average concentration of each component in time is shown in Figure 8. The monomer consumption rate, that is, the polymer generation rate, depends on the concentration of the propagating radical. Therefore, at the beginning

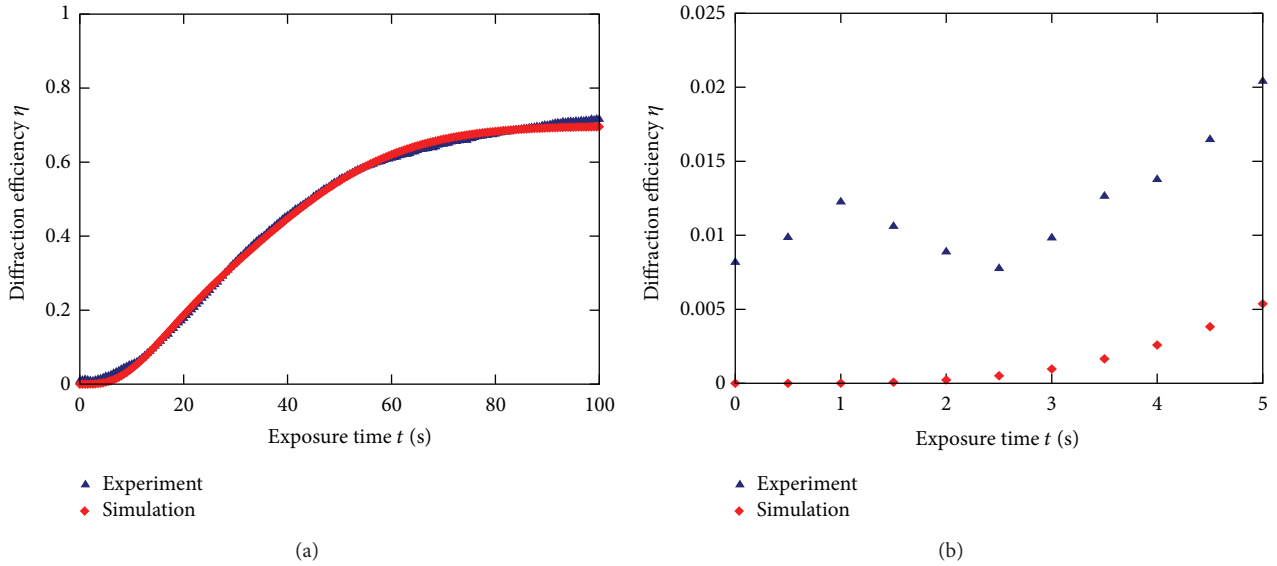

Figure 6: Time variation of diffraction efficiency.

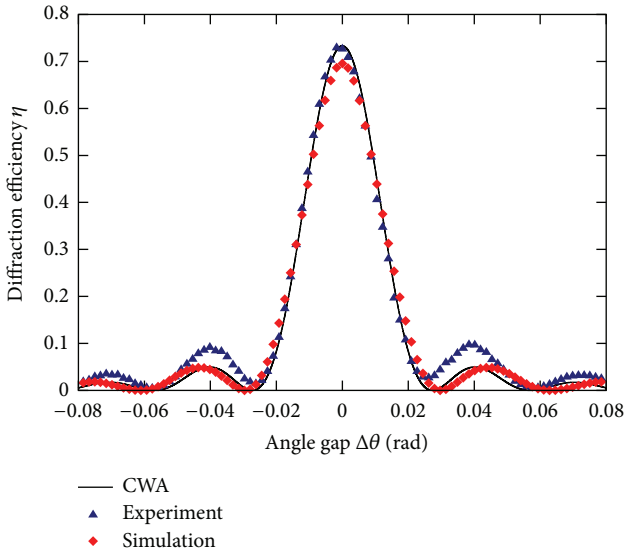

Figure 7: Angular selectivity.

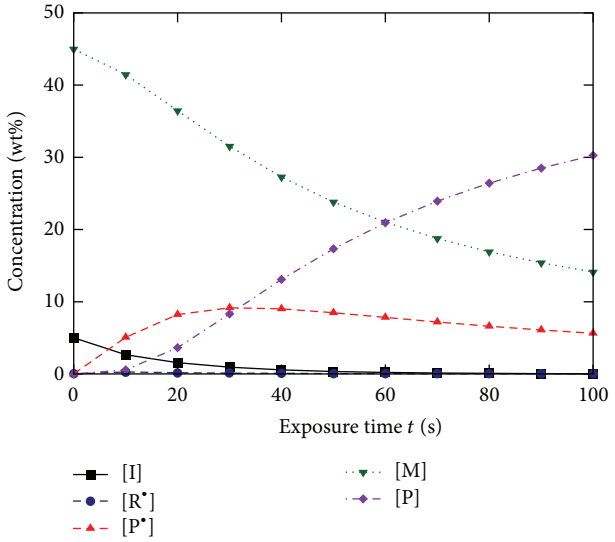

Figure 8: Time variation of the concentration.

of the exposure, the diffraction efficiency did not increase (Figure 6).

Figure 9 shows the time variation of the refractive index distribution. The horizontal axis is the x-coordinate normalized with the grating period Λ and the vertical axis is the refractive index n.

The results show that the higher harmonic components increase with exposure time. The higher harmonic components increase proportionally to the ratio between the diffusion coefficient and polymerization rate. The grating form can be approximated as Fourier series expansion:

$$n(x) = a_0 + \sum_{k=1}^{\infty} a_k \cos\left(\frac{2\pi}{\Lambda} kx\right). \quad (17)$$

Fourier coefficients a_k ($k \leq 10$) which is estimated from the simulation results are listed in Table 6.

As shown in the Table 6, the grating has high-harmonic components. The first higher harmonic component $a_1 = 6.343 \times 10^{-3}$ closes to $\Delta n = 6.018 \times 10^{-3}$ which is estimated from the experimental results with CWA. Consequently, the interdiffusion model can be used to estimate the medium parameters.

4. Conclusion

We simulated the formation of holographic gratings in photopolymers using the interdiffusion model. We considered the elementary reactions of initiation, propagation,

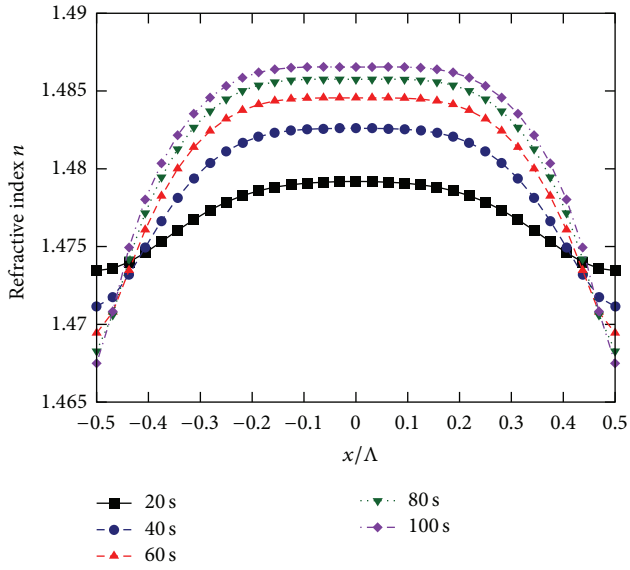

Figure 9: Refractive index distribution in time.

Table 6: Fourier coefficients.

k	a_k
0	1.483
1	6.343×10^{-3}
2	-3.467×10^{-3}
3	1.708×10^{-3}
4	-1.030×10^{-3}
5	6.774×10^{-4}
6	-4.702×10^{-4}
7	3.358×10^{-4}
8	-2.462×10^{-4}
9	1.828×10^{-4}
10	-1.388×10^{-4}

and termination. We analyzed the diffraction characteristics in detail by high-order BPM and estimated medium parameters, such as reaction rates and diffusion coefficients, with LMA. The proposed model and analytical methodology can be used to quantify the medium parameters. We believe that the results will provide useful information for developing holographic recording materials.

Conflict of Interests

The authors declare that there is no conflict of interests regarding the publication of this paper.

References

[1] G. Zhao and P. Mouroulis, "Diffusion model of hologram formation in dry photopolymer materials," *Journal of Modern Optics*, vol. 41, pp. 1929–1939, 1994.

[2] J. T. Sheridan and J. R. Lawrence, "Nonlocal-response diffusion model of holographic recording in photopolymer," *Journal of the Optical Society of America A*, vol. 17, no. 6, pp. 1108–1114, 2000.

[3] J. T. Sheridan, F. T. O'Neill, and J. V. Kelly, "Holographic data storage: optimized scheduling using the nonlocal polymerization-driven diffusion model," *Journal of the Optical Society of America B: Optical Physics*, vol. 21, no. 8, pp. 1443–1451, 2004.

[4] J. T. Sheridan, J. V. Kelly, M. R. Gleeson, C. E. Close, and F. T. O'Neill, "Optimized holographic data storage: diffusion and randomization," *Journal of Optics A: Pure and Applied Optics*, vol. 8, no. 3, pp. 236–243, 2006.

[5] H. M. Karpov, V. V. Obukhovsky, and T. N. Smirnova, "Generalized model of holographic recording in photopolymer materials," *Semiconductor Physics Quantum Electronics & Optoelectronics*, vol. 2, pp. 66–70, 1999.

[6] R. L. Sutherland, V. P. Tondiglia, L. V. Natarajan, and T. J. Bunning, "Phenomenological model of anisotropic volume hologram formation in liquid-crystal-photopolymer mixtures," *Journal of Applied Physics*, vol. 96, no. 2, pp. 951–965, 2004.

[7] J. V. Kelly, M. R. Gleeson, C. E. Close et al., "Temporal analysis of grating formation in photopolymer using the nonlocal polymerization-driven diffusion model," *Optics Express*, vol. 13, no. 18, pp. 6990–7004, 2005.

[8] V. L. Colvin, R. G. Larson, A. L. Harris, and M. L. Schilling, "Quantitative model of volume hologram formation in photopolymers," *Journal of Applied Physics*, vol. 81, no. 9, pp. 5913–5923, 1997.

[9] S. Piazzolla and B. K. Jenkins, "First-harmonic diffusion model for holographic grating formation in photopolymers," *Journal of the Optical Society of America B*, vol. 17, no. 7, pp. 1147–1157, 2000.

[10] C. E. Close, M. R. Gleeson, and J. T. Sheridan, "Monomer diffusion rates in photopolymer material. Part I. Low spatial frequency holographic gratings," *Journal of the Optical Society of America B: Optical Physics*, vol. 28, no. 4, pp. 658–666, 2011.

[11] C. E. Close, M. R. Gleeson, D. A. Mooney, and J. T. Sheridan, "Monomer diffusion rates in photopolymer material. Part II. High-frequency gratings and bulk diffusion," *Journal of the Optical Society of America B: Optical Physics*, vol. 28, no. 4, pp. 842–850, 2011.

[12] Y. Qi, H. Li, E. Tolstik et al., "Study of PQ/PMMA photopolymer. Part 1: theoretical modeling," *Journal of the Optical Society of America B: Optical Physics*, vol. 30, no. 12, pp. 3298–3307, 2013.

[13] Y. Qi, E. Tolstik, H. Li et al., "Study of PQ/PMMA photopolymer. Part 2: experimental results," *Journal of the Optical Society of America B*, vol. 30, no. 12, pp. 3308–3315, 2013.

[14] Y. Qi, E. Tolstik, H. Li et al., "Study of PQ/PMMA photopolymer. Part 2: experimental results," *Journal of the Optical Society of America B: Optical Physics*, vol. 30, no. 12, pp. 3308–3315, 2013.

[15] Y. Qi, H. Li, J. P. Fouassier, J. Lalevée, and J. T. Sheridan, "Comparison of a new photosensitizer with erythrosine B in an AA/PVA-based photopolymer material," *Applied Optics*, vol. 53, no. 6, pp. 1052–1062, 2014.

[16] Y. Chung and N. Dagli, "Assessment of finite difference beam propagation method," *IEEE Journal of Quantum Electronics*, vol. 26, no. 8, pp. 1335–1339, 1990.

[17] S. Yoshida and M. Yamamoto, "Analysis of diffraction characteristics of holographic grating in photopolymer films by beam propagation method," *Japanese Journal of Applied Physics*, vol. 48, no. 3, Article ID 03A027, 2009.

[18] S. Yoshida, M. Saitoh, N. Yoshida, and M. Yamamoto, "Analysis of multiplexed holograms recording by using a two-dimensional beam propagation method," *IEEE Transactions on Magnetics*, vol. 45, no. 5, pp. 2264–2267, 2009.

[19] F. Horn and R. Jackson, "General mass action kinetics," *Archive for Rational Mechanics and Analysis*, vol. 47, pp. 81–116, 1972.

[20] F. Horn, "Necessary and sufficient conditions for complex balancing in chemical kinetics," *Archive for Rational Mechanics and Analysis*, vol. 49, pp. 172–186, 1972.

[21] M. Feinberg, "Complex balancing in general kinetic systems," *Archive for Rational Mechanics and Analysis*, vol. 49, pp. 187–194, 1972.

[22] T. Anada, T. Hokazono, T. Hiraoka, J.-P. Hsu, T. M. Benson, and P. Sewell, "Very-wide-angle beam propagation methods for integrated optical circuits," *IEICE Transactions on Electronics*, vol. E82-C, no. 7, pp. 1154–1158, 1999.

[23] G. R. Hadley, "Transparent boundary condition for the beam propagation method," *IEEE Journal of Quantum Electronics*, vol. 28, no. 1, pp. 363–370, 1992.

[24] K. Levenberg, "A method for the solution of certain non-linear problems in least squares," *Quarterly of Applied Mathematics*, vol. 2, pp. 164–168, 1944.

[25] D. W. Marquardt, "An algorithm for least-squares estimation of nonlinear parameters," *Journal of the Society for Industrial and Applied Mathematics*, vol. 11, no. 2, pp. 431–441, 1963.

[26] W. H. Press, S. A. Teukolsky, W. T. Vetterling, and B. P. Flannery, *Numerical Recipes*, The Art of Scientific Computing, Cambridge University Press, Cambridge, UK, 3rd edition, 2007.

[27] T. Sabel and M. Zschocher, "Transition of refractive index contrast in course of grating growth," *Scientific Reports*, vol. 3, article 2552, 2013.

[28] H. Kogelnik, "Coupled wave theory for thick hologram gratings," *The Bell System Technical Journal*, vol. 48, no. 9, pp. 2909–2947, 1969.

[29] N. Uchida, "Calculation of diffraction efficiency in hologram gratings attenuated along the direction perpendicular to the grating vector," *Journal of the Optical Society of America*, vol. 63, no. 3, pp. 280–287, 1973.